Autonomous basin climbing method with sampling of multiple transition pathways: application to anisotropic diffusion of point defects in hcp Zr

2014 J. Phys.: Condens. Matter 26 365402

(http://iopscience.iop.org/0953-8984/26/36/365402)

IOP Publishing Journal of Physics: Condensed Matter
J. Phys.: Condens. Matter **26** (2014) 365402 (16pp) doi:10.1088/0953-8984/26/36/365402

Autonomous basin climbing method with sampling of multiple transition pathways: application to anisotropic diffusion of point defects in hcp Zr

Yue Fan[1,3], Sidney Yip[1,2] and Bilge Yildiz[1]

[1] Department of Nuclear Science and Engineering, Massachusetts Institute of Technology, 77 Massachusetts Avenue, Cambridge, MA 02139, USA
[2] Department of Materials Science and Engineering, Massachusetts Institute of Technology, 77 Massachusetts Avenue, Cambridge, MA 02139, USA
[3] Materials Science and Technology Division, Oak Ridge National Laboratory, Oak Ridge, Tennessee 37831, USA

E-mail: byildiz@mit.edu

Received 18 June 2014
Accepted for publication 15 July 2014
Published 19 August 2014

Abstract

This paper presents an extension of the autonomous basin climbing (ABC) method, an atomistic activation-relaxation technique for sampling transition-state pathways. The extended algorithm (ABC-E) allows the sampling of multiple transition pathways from a given minimum, with the additional feature of identifying the pathways in the order of increasing activation barriers, thereby prioritizing them according to their importance in the kinetics. Combined with on-the-fly kinetic Monte Carlo calculations, the method is applied to simulate the anisotropic diffusion of point defects in hcp Zr. Multiple migration mechanisms are identified for both the interstitials and vacancies, and benchmarked against results from other methods in the literature. The self-interstitial atom (SIA) diffusion kinetics shows a maximum anisotropy at intermediate temperatures (400~700 K), a non-monotonic behavior that we explain to originate from the stabilities and migration mechanisms associated with different SIA sites. The accuracy of the ABC-E calculations is validated, in part, by the existing results in the literature for point defect diffusion in hcp Zr, and by benchmarking against analytical results on a hypothetical rough-energy landscape. Lastly, sampling prioritization and computational efficiency are demonstrated through a direct comparison between the ABC-E and the activation relaxation technique.

Keywords: atomistic simulation, potential energy landscape, defect migration pathways

(Some figures may appear in colour only in the online journal)

1. Introduction

Materials performance and degradation are significantly affected by the evolution of defect structures over long time scales [1]. Computational modeling and simulation have become an effective and widely established quantitative approach to studying materials, and can constructively complement the theoretical and experimental methods [2]. However, there is still a formidable challenge to predict material behavior over experimental time scales with traditional atomistic simulations. Although the aging of materials takes place in the time scale of years (~10^7 s [3]), the most widely used atomistic technique, molecular dynamics (MD) simulation, can hardly go beyond nano seconds (~10^{-9} s).

Properties of condensed matter rely on interaction between the atoms in the system, governed by the landscape of the

potential energy surface (PES [4]). Several atomistic simulation methods have been developed based on biased dynamics and the concept of escaping from deep-energy minima on the PES in static calculations to effectively capture events that would take place over long periods. The family of biased dynamics techniques include hyperdynamics [5–7] and temperature-accelerated dynamics (TAD [8]) methods, to boost the rare event transition. In hyperdynamics, a biased potential ΔV is added on the system's PES, and the transition can be boosted by a factor of $\exp[\Delta V/k_BT]$. The TAD method speeds up the transitions by increasing the temperature, and then extrapolates to a low-temperature regime, following the Arrhenius behavior, while filtering out the transitions that should not have occurred at the required temperature. Although the hyperdynamics method especially can be very accurate, there are computational challenges in the implementation of the bias potential—i.e. the bias potential must be zero at the dividing surfaces between the minima, and the identification of this bias form requires very high computational load. Recently, significant improvements have been made in calculating the bias potential more efficiently using the adaptive boost (AB) method [9, 10].

Static approaches that evolve the system on its PES include activation relaxation technique (ART [11, 12]), Dimer method [13], and autonomous basin climbing (ABC) method [14]. In both the ART and Dimer methods, multiple transition pathways associated with a given minimum-energy state can be captured, and this is performed by introducing perturbations to the initial state along different directions. Since the perturbations are randomly induced, the activation energies for the identified transitions also appear in a random order in this search. All the observed transitions are stored in the reaction catalogue, which serves as the input parameters for the following kinetic Monte Carlo (kMC) simulation [15–18]. The ART and Dimer method have been successfully applied to a series of studies, including the diffusion of point defects [13, 15–19], heat release from ion-implanted amorphous Si during its relaxation [20], and the plastic flow in glassy materials [21]. However, these methods may face unaffordable computation loads when simulating complex systems with many competing events during the material evolution. The reason is that for a complex non-equilibrium process, each minimum energy state is connected to many other states, each new observed state is connected to more states, and so on. Therefore, such a breadth-first search algorithm can easily become very expensive computationally. For example, in a recent study on the annihilation of a dislocation-dipole [22], Wang *et al* showed that the ART could not drive the system to the final state due to the 'very high computational load', and had to employ the ABC method to observe the dipole dissociation processes.

The ABC algorithm is also based on the activation-relaxation procedure, and explores and reconstructs the system's potential energy surface. It was developed by Kushima *et al* in computing the viscosity of supercooled liquids [14], and is inspired by Laio and Parrinello's idea of escaping from the free-energy minima [23]. By adding a series of penalty functions into the given basin on the PES, the ABC algorithm evolves the system along the pathway that has the lowest energy barrier without prior assumption of the reaction coordinates. This feature enables the ABC method to capture the dominant pathways of system evolution, where the states are connected in series over a 1D chain. Recently, Cao *et al* further optimized the ABC method by introducing a self-learning algorithm [24], which can significantly reduce the computational cost. The implementation of the ABC algorithm is technically straightforward, and has been demonstrated to accurately capture the mechanism and kinetics of a series of unit processes, including the unfaulting of a self-interstitial atom (SIA) cluster in bcc Fe [25], the structure of a vacancy cluster in fcc Al [26], and the dislocation motion and structure [22, 27] and interaction of dislocation with obstacles in both hcp Zr and bcc Fe [28, 29]. However, when there are multiple competitive processes simultaneously, because of the 1D nature of the system evolution, the original ABC method overestimates the system evolution time [30–32]. This paper extends the ABC algorithm so that it can now capture multiple competing transition pathways from each minimum energy state explored on the PES.

In this paper, we discuss the underlying reason for overestimating the evolution time by comparing the original ABC method with analytical transition state theory (TST) and kMC results. We describe the new algorithm that extends ABC (ABC-E) to capture multiple transition pathways from an individual basin on the PES. The ABC-E algorithm is benchmarked against the analytical results on a hypothetical rough PES. We also demonstrate the prioritization of sampled paths by ABC-E and the relative computational efficiency by comparing the ABC-E method and ART in the simulation of vacancy migration in hcp Zr.

ABC-E and kMC calculations are employed to simulate the point defect diffusion in an anisotropic material, hcp Zr. Point defect diffusion is important in governing the evolution of microstructure in Zr alloys, which are widely used as cladding materials of nuclear fuel in light water reactors (LWR [33]). For safety and operational purposes, it is important to be able to predict the mechanical properties of Zr, which are largely dependent on the defect evolutions [34–39]. Furthermore, the point defect diffusion in hcp Zr is an ideal problem to test the accuracy of the new algorithm, ABC-E, because the diffusion of vacancies and interstitials can take place via dissimilar migration paths and sites in this structure. The results show that ABC-E samples effectively multiple inequivalent transition pathways for the migration of point defects in hcp Zr. The extent of anisotropy in the diffusivity of point defects is assessed as a function of temperature. We find that the SIA diffusion exhibits a non-monotonic behavior of isotropic-anisotropic-isotropic transitions with increasing temperature. This behavior originates from different stabilities and migration mechanisms associated with different SIA sites when using the MA07 interatomic potential [40]. This result is in contrast to previous findings using a different potential [41], because the two potentials provide different relative stabilities of the SIA sites.

2. Methodology

As noted above, it is possible that the original ABC method can overestimate the system evolution time scale in the case

of multiple competitive processes [30–32]. In this section we introduce the underlying reason for the time overestimation by comparing the ABC method with analytical TST and kMC results. Then we modify the ABC algorithm to ABC-E to capture multiple transition pathways from an individual basin on the PES. This extension significantly improves the accuracy of the calculated time of evolution. A very brief summary of the result of ABC-E in comparison to ABC and analytical TST was recently reported [32]. Here we provide the description of the new algorithm and its comparison to TST in detail.

2.1. Transition state theory and full catalogue kinetic monte carlo method

For a given transition network, according to TST, the evolution time from the initial ('*i*' in figure 1) to the final state ('*f*' in figure 1) can be calculated as the following:

If state p and q are connected with each other, following TST, the jump frequency from p to q can be derived by:

$$k_{p,q} = k_0 \exp\left[-\frac{E_{p,q}}{k_B T}\right], \tag{1}$$

where the prefactor k_0 is the attempt frequency, and $E_{p,q}$ is the activation energy from state p to q. The residence time from state p is given by:

$$\tau_p = \frac{1}{k_{p,1} + k_{p,2} + \cdots + k_{p,n(p)}}, \tag{2}$$

where $n(p)$ is the number of neighboring nodes connected with state p.

The evolution time from i to f can therefore be calculated as:

$$t_{i\to f} = \tau_i + \frac{k_{i,1}}{k_{i,1} + \cdots + k_{i,n(i)}} t_{1\to f} + \cdots + \frac{k_{i,n(i)}}{k_{i,1} + \cdots + k_{i,n(i)}} t_{n(i)\to f}, \tag{3}$$

and similarly, for other unknown variables such as $t_{1\to f}$, the definition follows:

$$t_{1\to f} = \tau_1 + \frac{k_{1,i}}{k_{1,i} + \cdots + k_{1,n(1)}} t_{i\to f} + \cdots + \frac{k_{1,n(1)}}{k_{1,i} + \cdots + k_{1,n(1)}} t_{n(1)\to f}. \tag{4}$$

We can rewrite the above equations into the matrix expression as below:

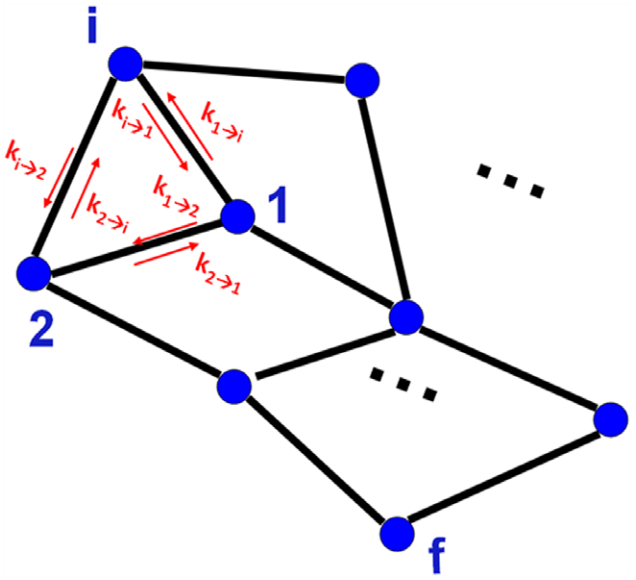

Figure 1. Illustration of the system evolution from one minimum energy state to another on the PES in the form of a nodal network, with the initial state '*i*' and the final state '*f*'.

The evolution time $t_{i\to f}$ can be analytically derived by diagonalizing the $n*n$ matrix above, where n is the number of nodes in the system. In reality, the dimension n can be very large, which makes the analytical solution very difficult to obtain. Therefore, kMC [42–44] is widely employed to get the approximated numerical solution. The more transition states are explored, the higher the accuracy of the kMC simulations [42]. Therefore, algorithms that can efficiently identify the important transition pathways and corresponding energy barriers are desirable. As stated earlier, the aim of the present work is to improve the capabilities of the ABC algorithm. The original ABC method is inherently most likely to capture only the dominant transitions in a 1D chain (shown below). This approach was proven successful, especially in finding the governing mechanism in the evolution of non-equilibrium systems. On the other hand, in a system whose evolution is described by competing processes, the original ABC algorithm is not sufficient to describe the true kinetics. To overcome this challenge, we penalize the system from the same basin multiple times in the original ABC framework, while blocking the observed transitions. This new algorithm, ABC-E, is then able to capture arbitrarily more transition states (seen below), thereby building the rate catalog as accurately as possible for kMC simulations.

$$\begin{pmatrix} 1 & -\frac{k_{i,1}}{k_{i,1}+\cdots k_{i,n(i)}} & \cdots & -\frac{k_{i,n(i)}}{k_{i,1}+\cdots k_{i,n(i)}} & \cdots & 0 \\ \frac{k_{1,i}}{k_{1,i}+\cdots+k_{1,n(1)}} & -1 & \cdots & \frac{k_{1,n(1)}}{k_{1,i}+\cdots+k_{1,n(1)}} & \cdots & 0 \\ \vdots & & \cdots & \ddots & & 0 \\ & & & & & \vdots \end{pmatrix} \bullet \begin{pmatrix} t_{i\to f} \\ t_{1\to f} \\ \vdots \\ \vdots \end{pmatrix} = \begin{pmatrix} \tau_i \\ -\tau_1 \\ \vdots \\ \vdots \end{pmatrix}. \tag{5}$$

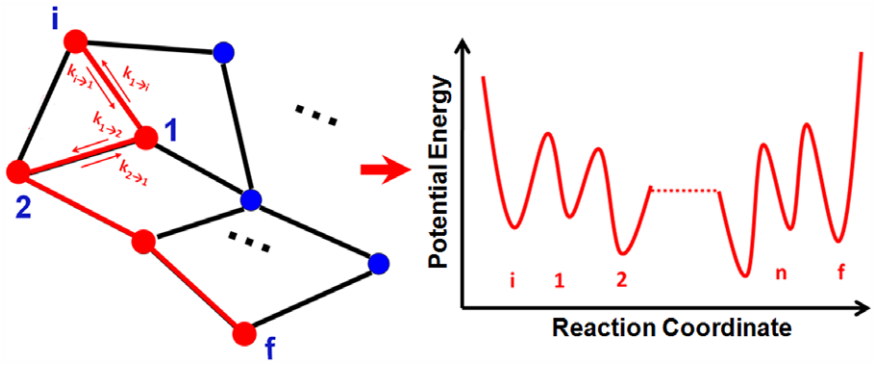

Figure 2. Illustration of the system evolution from one minimum energy state to another on the PES in the form of a nodal network, with the initial state '*i*' and the final state '*f*'. The collection of states and connectivities are the same as in figure 1. An evolution chain is provided by the ABC algorithm as the red path on the left, corresponding to the PES of a 1D chain of transitions illustrated on the right.

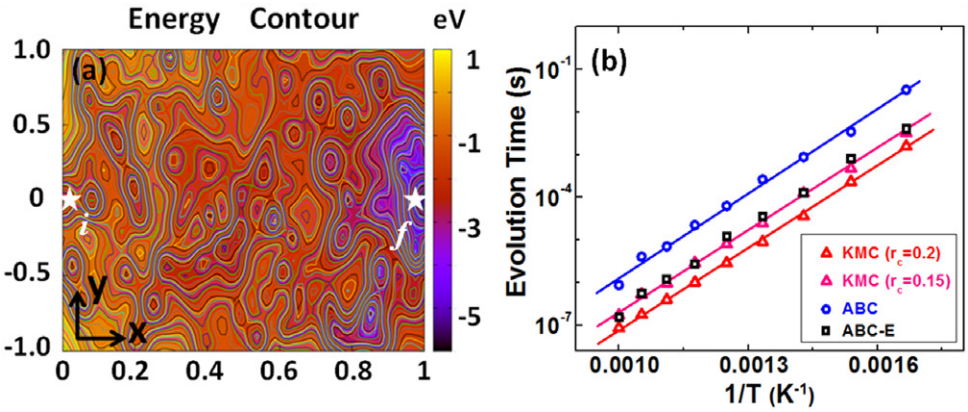

Figure 3. (*a*) (Adapted with permission from [32]). A pre-constructed 2D PES with a rough landscape, for representing the system evolution from *i* to *f* with multiple competing processes. (*b*) A variation of the evolution time with temperature sampled by full-catalog kMC (with two different r_c), ABC, and ABC-E.

2.2. The 1D nature of the original ABC algorithm

Now let's revisit the transition network discussed above with the original ABC method. The ABC algorithm evolves the system mainly towards the pathway with the lowest barrier, while neglecting other, higher-barrier pathways. Therefore, for the same system, ABC will provide an evolution chain that connects the transition paths in 1D instead of a network (seen in figure 2).

Since for this 1D chain, each state is only connected with one state before it and one state after on the nodal network of states, the residence time for state p is given by:

$$\tau_p = \frac{1}{k_{p,p-1} + k_{p,p+1}} \tag{6}$$

And similarly, the evolution time from i to f can be calculated by solving the following linear equations:

$$\begin{pmatrix} 1 & -1 & 0 & 0 & \cdots & 0 \\ \frac{k_{1,i}}{k_{1,i}+k_{1,2}} & -1 & \frac{k_{1,2}}{k_{1,i}+k_{1,2}} & 0 & \cdots & 0 \\ 0 & \frac{k_{2,1}}{k_{2,1}+k_{2,3}} & -1 & \frac{k_{2,3}}{k_{2,1}+k_{2,3}} & \cdots & 0 \\ \vdots & & & \ddots & & \vdots \\ 0 & 0 & \cdots & 0 & \frac{k_{n,n-1}}{k_{n,n-1}+k_{n,f}} & -1 \end{pmatrix} \bullet \begin{pmatrix} t_{i\to f} \\ t_{1\to f} \\ \vdots \\ t_{n\to f} \end{pmatrix} = \begin{pmatrix} \tau_i \\ -\tau_1 \\ \vdots \\ -\tau_n \end{pmatrix}. \tag{7}$$

The dimension for the above matrix is the length of the 1D chain, which is significantly smaller than the total number of nodes in the system. In addition, the matrix has the banded tridiagonal structure, which is much simpler than the matrix in the last section for a full catalog of events and transitions. kMC can also be employed based on this reduced matrix to calculate the evolution time $t_{i\to f}$. Because of the reduced dimension and simpler underlying mathematical structure, the ABC-based kMC method saves substantial computational load compared to the full-catalog kMC calculations.

Despite the successful implementation of the original ABC method in a series of studies on different unit processes [14, 25–27, 45–47], the 1D nature of the ABC method can lead to an overestimation of the system evolution time [30–32] if there are multiple competitive processes governing the system evolution. To give an illustration we consider a synthetic

comparison between ABC and full catalogue kMC using a pre-constructed hypothetical 2D PES (figure 3(*a*)). To simulate a scenario with multiple processes, we randomly introduced 100 intermediate minima with varying depths and widths (figure 3(*a*)) to form a rough energy landscape connecting the initial and final states. In the kMC simulations, the transition catalog is defined by a cut-off radius r_c. In other words, if the distance between two minima is smaller than r_c, then the two states are defined as connected and a direct transition between them is allowed. In the kMC simulations, for a state with residence time τ, a random number between 0 and 1 is generated during each step, and the time is preceded by the amount $-\tau/\ln(\mu)$, following the kMC convention [42–44]. Note that r_c is an empirically chosen parameter in kMC simulations, and below we demonstrate the effect of the choice of r_c in the quantitative results. A 1D trajectory of events describing the evolution from the same prescribed initial state to the final state was found using ABC calculations; this was used to estimate the temperature-dependent system evolution time and the effective activation energy in the kMC method, statistically averaged over hundreds of simulations.

As shown by the Arrhenius plot in figure 3(*b*), the slope of the ABC results is identical to the full-catalog kMC results, which indicates that both results give the same effective barrier. This demonstrates that ABC is providing the dominant transition pathway. On the other hand, the evolution time in ABC results is overestimated by about two orders of magnitude, in this case compared to kMC with $r_c = 0.2$. This results from the 1D nature of the original ABC algorithm, because the residence time at each state, as introduced above, is governed by $1/(k_{\text{forward}} + k_{\text{backward}})$, whereas in kMC simulations using a full catalog of transition pathways, it is governed by $1 / \sum k_i$. Therefore, the evolution time calculated by the ABC method for a scenario with multiple competing processes can be overestimated here because $1 / (k_{\text{forward}} + k_{\text{backward}}) > 1 / \sum k_i$. On the other hand, the magnitude of the overestimation by ABC compared to kMC simulations also depends on the accuracy of the full-catalog kMC results with a selected value of r_c. We show two kMC results in figure 3(*b*) with different cut-off radii of 0.2 and 0.15. For the larger cut-off radius, the transition catalog is more extensive than for the smaller cut-off radius, and thus, yields a faster evolution time. However, this does not mean that all the events sampled with the larger r_c are directly connected to the original state, and if r_c is too large, the simulation might include unphysical transitions. Regardless of the precise accuracy of the kMC method, the comparison in figure 3(*b*) demonstrates that the time overestimation in the original ABC algorithm is due to the 1D nature of the identified transitions, rather than an inherent limitation of finding the dominant pathway.

In particular for non-equilibrium processes, the ABC method has been shown to be able to find the governing evolution pathways. For instance, in our recent work [29] in simulating dislocation-defect interactions in metals as a function of strain rate and temperature, it is demonstrated that ABC gives exactly the same mechanism and kinetics as MD simulations in the fast strain-rate regime, and in the slow strain-rate regime, it gives results that are credible and consistent with experiments. Another recent study by Wang, *et al* [22] on the annihilation of dislocation dipoles also shows that ABC could well explain the observations from experiments. In another example simulating the vacancy-clustering process, both ABC [31] and k-ART [30] give the void nucleation and growth behavior similarly, and the key difference is the time scales predicted by the two methods. (ABC as the one overestimating the timescale.)

2.3. Extension of the ABC (ABC-E) method to sample multiple transition pathways

To address the concern over the time overestimation explained above, the ABC method is modified by the following algorithm to sample multiple transition pathways in the system evolution:

1. For a given initial state, apply the original ABC algorithm steps until the first neighboring state is observed. Each original ABC step consists of two stages—activation and relaxation. During the activation stage, a penalty function in Gaussian form [14] is added into the given basin on PES. The activation is then followed by a relaxation stage to minimize the energy of the system. In the examples studied in this work, each relaxation stage consists of 500 force evaluations through the steepest descent method.
2. Record the new state, and put the system back to the previous state.
3. Add a blocking penalty function (also in Gaussian form) on the previously observed saddle point. The detailed parameters of the blocking penalty function are shown in the beginning of section 3 for the studied system in this paper.
4. Implement regular ABC steps until the next new minimum energy state is observed.
5. Judge whether a new state or a previously visited state is found: (a) if it is a previously visited state, then put the system back to the previous state, and add an additional blocking function on the saddle point; restart step 4. (b) if it's a new state, go to step 2.
6. A note on finding the activation energy barrier values: in principle, the minimized energy just before the system escapes into a new minimum energy state represents the energy of the saddle point. The energy difference between the saddle point and the initial minimum state is the activation energy for that particular pathway. However, because of the penalty functions, the activation energy can be overestimated in the ABC or ABC-E methods. We take the pathways (i.e. mechanisms) identified by steps 1–5 above. To enable better accuracy in the computation of kinetics based on those pathways, we employ the nudged elastic band method to calculate the precise values of activation energies connecting these pathways determined by ABC-E.

By doing so, a series of states that neighbor the original state are found. The order of finding these new states is with

increasing activation barriers. The more the identified transitions, the more accurate the results. The criteria for stopping the search for more states can be defined in two ways. An easy criterion is to set a maximum number of total penalty functions to be added to the entire simulation in steps 1–5 described above, N_{steps}^{MAX}, and consider all the identified transition pathways within this upper bound of search steps. Specifically, let us denote n_1 as the number of penalty functions added before detecting the first connected state to the original minimum. Once the first connected state is found, the system is set back to the original state, following the procedures explained above. Let us assume it then takes another n_2 steps to find the second connected state to the original minimum-energy state. The search is terminated after observing the i_{th} state, such that $\sum_{j=1}^{j=i} n_j \leq N_{steps}^{MAX} < \sum_{j=1}^{j=i+1} n_j$, where n_j represents the number of ABC steps in the search for the jth state. This criterion is suitable for situations in which there are not too many different transition states, because under such a circumstance, a reasonable choice of N_{steps}^{MAX} can be enough to search the complete transition states. For example, our experiences on a hypothetical 2D PES and on the anisotropic diffusion of point defects in Zr (discussed in the next section) suggest that assuming N_{steps}^{MAX} to be in the order of a few hundred is sufficient to get converged results.

A second criterion can be defined by the following. We assume the number of the already-observed states is N_{states}^{obs}, with the associated barriers, from low to high, as E_1^{obs}, E_2^{obs}, …, $E_{N_{states}^{obs}}^{obs}$. Once a new state is found with the barrier E^{new}, we compare the relative probability of this transition with respect to the previously observed states at a given temperature by calculating

$$\alpha(T) = \frac{\exp\left(-E^{\text{new}}/k_BT\right)}{\sum_{N_{\text{states}}^{\text{obs}}} \exp\left(-E_i^{\text{obs}}/k_BT\right)}. \tag{8}$$

If the calculated $\alpha(T)$ is very small, which means the new state has only negligible probability to be visited, then the search process can be terminated. The rule of thumb for the specific value of $\alpha(T)$, following other, similar truncation criteria used in the TAD [8] and kinetic-ART [18] methods, is around 0.1%.

The extension of the original ABC method, now called ABC-E, is further implemented into the on-the-fly kMC framework to more accurately estimate the kinetics of system evolution. We revisit the same benchmark problem on the 2D hypothetical PES, now sampled by ABC-E over hundreds of kMC simulations, and the results are shown in figure 3(*b*). It can be seen that the results of ABC-E show a much better numerical accuracy compared to the full-catalog kMC simulations, as expected.

We would like to stress that, in terms of searching multiple transition paths, the ABC-E method is similar to ART and the Dimer method in that it can handle a growing amount of states and pathways. However, there are noticeable differences between them. A detailed comparison between the ABC-E method and ART is shown later in section 5. Briefly, in ART and the Dimer method, once a transition pathway is captured, the system is set back to the original state and displaced along different *random* directions to find other transition pathways associated with the given minimum state. On the other hand, in the ABC-E framework, since the system prefers to evolve towards the lowest available saddle point, the order of observed transition states is with increasing activation barrier. In practice, it is possible that ABC-E finds a transition with a higher barrier before the one with a lower barrier (i.e. a reverse-order problem) when the saddle points energy differences are quite small compared with the penalty energy parameter used in ABC-E. Overall, however, we observe the general increasing trend in the barrier heights, as shown in section 5. This algorithm therefore prioritizes the important transitions. And this feature can help ABC-E build the important transition catalog more efficiently.

As demonstrated in section 5, during the sampling process, we observe two additional features that make ABC-E appealing in practice. First, in ABC-E, different searches are not completely independent of each other. In contrast, once the first pathway is observed, the successive searches do not start from the very bottom of the basin. Instead, the successive searches start from the current level of the partially filled basin. Not having to start each search from the bottom of the basin makes the sampling of transition pathways more efficient, as the observed pathways increase. Second, by blocking the visited saddle points, ABC-E can effectively prevent the observed transitions from being found many times. Such a decrease in redundancy rate therefore increases the sampling efficiency. For example, Malek *et al* show that [48], a lot of pathways are found multiple times in ART, and the redundancy probability is about 68.6%–92.9%, depending on the parameters used in ART. In the ABC-E method, since the observed saddle points are blocked by the penalty function, the redundancy rate is much lower. We would like to stress that the efficiencies of different methods largely depend on the parameters used and the system at hand, and that different modeling techniques have their own advantages for different types of problems. A more thorough comparison between different techniques is warranted in the future.

3. Migration mechanisms of point defects in hcp Zr

Hcp Zr is an anisotropic material, and there are multiple inequivalent transition pathways on which the point defects can migrate. For example, there are two migration paths for vacancy diffusion, one on the basal plane and one out of the basal plane. Self-interstitial atom (SIA) migration has many more pathways in hcp Zr compared to vacancy migration. It is impossible for the original ABC method to capture all possible migration mechanisms because it can only provide the lowest-barrier mechanism and would inaccurately estimate the diffusion kinetics of point defects in Zr. In this section, we employ ABC-E to simulate the anisotropic diffusivities of vacancy and SIA in Zr. The migration mechanisms and the corresponding activation energy barriers of point defects

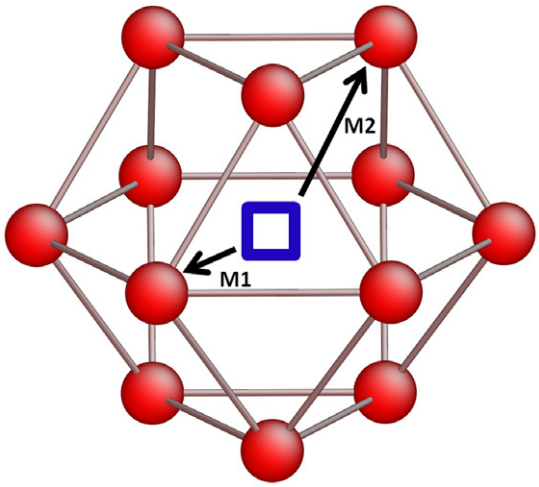

Figure 4. The in-plane (M1) and out-of-plane (M2) migration paths for a Zr vacancy in the hcp crystal. Both of these paths are captured by the ABC-E algorithm sequentially. The red spheres represent the atoms on the lattice points, while the blue square represents the missing atom—i.e. the vacancy.

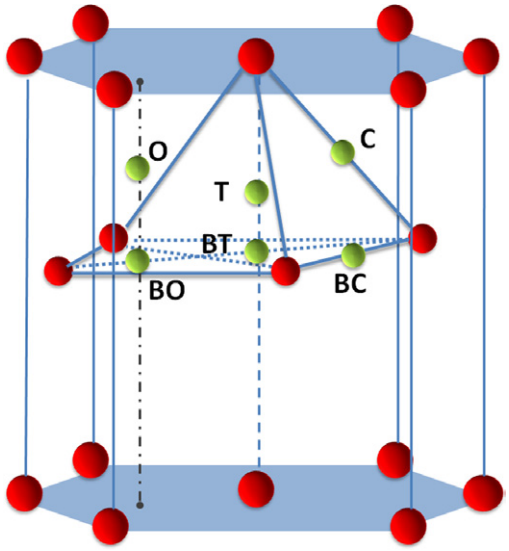

Figure 5. Six possible interstitial sites in a hcp crystal, shown by green spheres. The red spheres represent the atoms on the lattice points.

are identified by ABC-E, and they are, in part, benchmarked consistently with other methods reported in literature. The transition pathways and energy barriers are then input into on-the-fly kMC simulations to study the anisotropic diffusion kinetics of point defects in Zr. An interesting behavior for the SIA diffusion was found: specifically, a non-linear isotropic-anisotropic-isotropic transition in diffusivities with increasing temperature has been observed, arising from the temperature dependence of the stable SIA structure.

The dimension of the simulation cell is 38.8A*39.2A*41.3A, containing 2688 Zr atoms. To simulate the vacancy, an atom is extracted from the bulk, while for SIA an extra atom is inserted into the system. Periodic boundary conditions are applied for all directions. A recent embedded atom method (EAM) potential developed by Mendelev *et al* [40] (MA07) is employed. For vacancy migrations, penalty parameters of 0.5 eV, 0.25 A^2 (for both the regular bias filling function and the blocking function) are employed in ABC-E. For SIA migrations, penalty parameters of 0.01 eV and 0.05 A^2 are employed in ABC-E.

3.1. Vacancy migration pathways

By employing the ABC-E method, we observed two migration mechanisms for vacancy diffusion—i.e. in the basal plane and out of the basal plane. The in-plane migration (M1) had a lower barrier 0.68 eV compared to the out-of-plane migration (M2), which had a 0.76 eV barrier. Both migration paths had a degeneracy of six. The derived mechanisms and barriers are consistent with other results reported independently by Subramanian *et al* using TAD simulations [49].

3.2. SIA migration pathways

The migration of a SIA in Zr is much more complicated than that of a vacancy since the SIA can exist at different interstitial sites. Here we consider six possible interstitial sites based on the geometry of hcp crystals. These are the octahedral (O), basal octahedral (BO), tetrahedral (T), basal tetrahedral (BT), crowdion (C), and basal crowdion (BC), as shown in figure 5. According to previously reported DFT calculations [50, 51], the split (S) configuration is another candidate site for the interstitial. However, these S structures are very unstable [49] and can exist in multiple slightly different configurations, which makes the assessment uncertain [49, 52]. Therefore, we did not consider the S site in the analysis.

To check the stabilities based on formation energies for an SIA at these interstitial sites, we insert an extra atom into each interstitial site (one at a time) and then relax the system by the steepest descent algorithm. It can be seen in figure 6 that, among the six interstitial sites, only three stable structures arise. Both the perfect O and C sites decay to a distorted O site with the degeneracy of six. Both the T and BT sites are unstable and decay to the BC site. The BO site is energetically stable.

The energetics for these sites with the MA07 potential are summarized in table 1 below. We define the formation energy of an SIA at different sites as:

$$E_f^{SIA} = E_{tot}^{N+1} - \frac{N+1}{N} \cdot E_{perfect}^{N},$$

where E_{tot}^{N+1} represents the total potential energy of the system, including the SIA, while $E_{perfect}^{N}$ is the potential energy of a perfect hcp Zr system containing N atoms.

The distorted O site is relatively more stable, with the formation energy of 2.74 eV. The formation energies for the BC and BO sites are 2.83 eV and 2.86 eV, respectively. The relative stability of the O site is consistent with previous works using the same potential [40, 53] and several DFT calculations [50, 51]. However, the quantitative results differ, and the discrepancies might arise from the size of simulation cells used in various reports [50, 51, 53, 54]. It is notable that all three

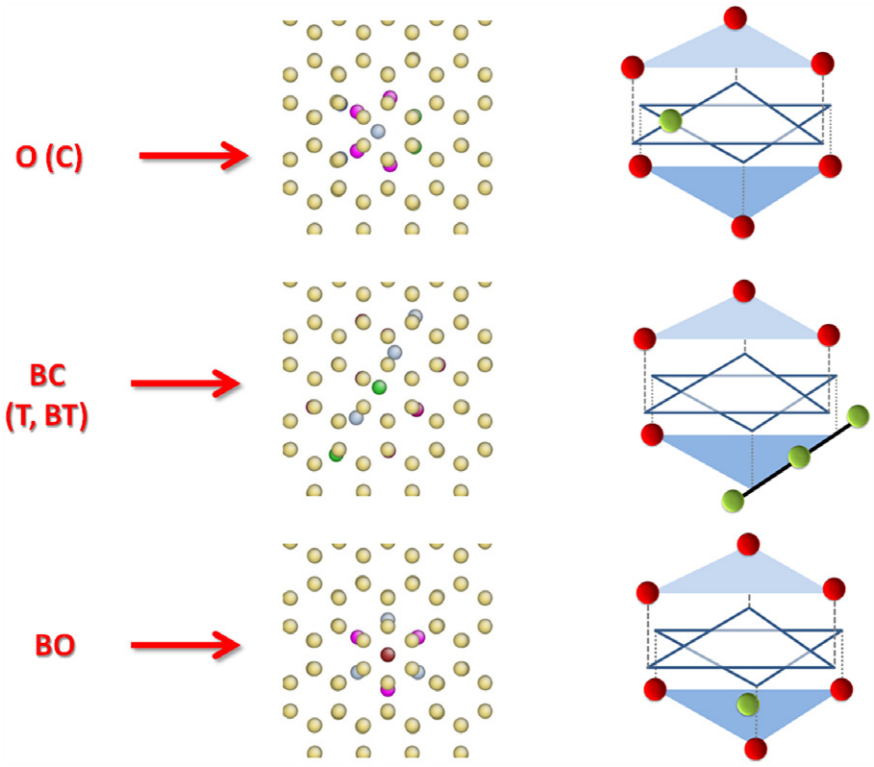

Figure 6. Only three stable SIA sites, O, BC, and BO, are found to be stable in hcp Zr, among all the six possible geometric sites surveyed using the MA07 interatomic potential.

Table 1. The formation energy of the SIA states in hcp Zr, and the comparison against previously reported results using the same MA07 potential.

SIA state	Current study (eV)	Mendelev *et al* [40] (eV)	Khater *et al* [53] (eV)
O	2.74	2.88	2.78
BO	2.86	2.90	N/A
BC	2.83	2.91	N/A

SIA sites have comparable energies, and therefore SIAs are expected to be present comparably at all of these three sites at elevated temperatures.

We identified the migration mechanisms and the corresponding activation energies of SIA diffusion in hcp Zr using the ABC-E method. Two key mechanisms describe the migration of SIA: the O-mechanism and the BC-mechanism, respectively.

1. O-mechanism
   Starting from the O state (as shown in figure 6), there are mainly three migration pathways.

(1.a) *Direct O-O hopping*. As shown in figure 7 below, the O state SIA directly migrates to the 1st and 2nd nearest neighbor (NN) O states, with the migration barriers of 0.028 eV and 0.062 eV, respectively.

(1.b) *O-M1-BC migration.* As shown in figure 8 below, the SIA in the O state first moves away from the middle plane and evolves to a middle state M1, where the extra atom stays slightly above the basal plane. Then the SIA moves further downward to the basal plane and forms the BC state. Although figure 8 shows only one pathway of O-M1-BC, the O-M1 transition actually has a degeneracy of two, i.e. the SIA can move either upward or downward, and eventually leads to two BC states on different basal planes. The associated migration barriers are also marked in the figure. The effective barrier from O state to BC state is about 0.13 eV, while the effective barrier from BC state to O state is around 0.04 eV. It can be seen that M1 is quite unstable due to the small transition barriers to either O or BC state.

(1.c) *O-M2-O migration*. The O-M2-O migration is an interstitialcy mechanism. As shown in figure 9 below, the extra atom in O state first moves away from the middle plane and forms a dumbbell (M2) with the nearest atom in the basal plane. (This M2 is actually the split configuration [49, 52].) Then the nearest atom is pushed to an O state in another unit cell. The degeneracy for the O-M2 transition is two since there are two nearest-neighbor atoms to the SIA. The corresponding migration barriers are also marked in the figure. The effective barrier for this interstitialcy mechanism is around 0.1 eV. It can also be seen that M2 is an unstable state due to the very shallow minimum.

2. BC mechanism
   Starting from the BC state (as shown in figure 6), we observe three migration pathways.

(2.a) *BC-BC glide motion*. Since BC is in crowdion structure, it easily glides with a low migration barrier 0.013 eV. The 1D glide motion has a degeneracy of two.

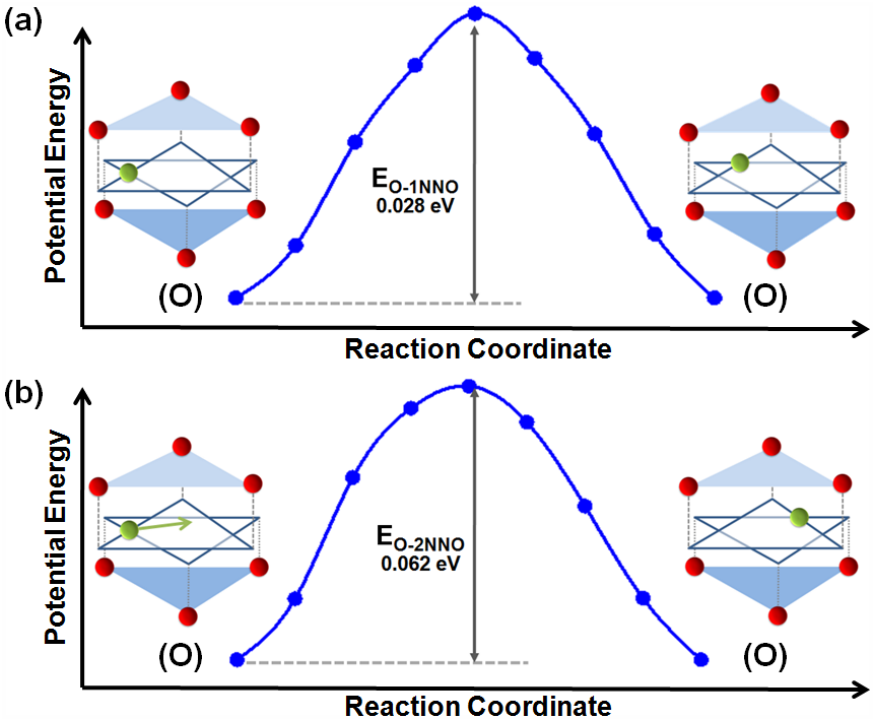

Figure 7. Direct O-O hopping mechanism. O state can migrate to either the 1st NN O state or the 2nd NN O state, as shown in (*a*) and (*b*), respectively.

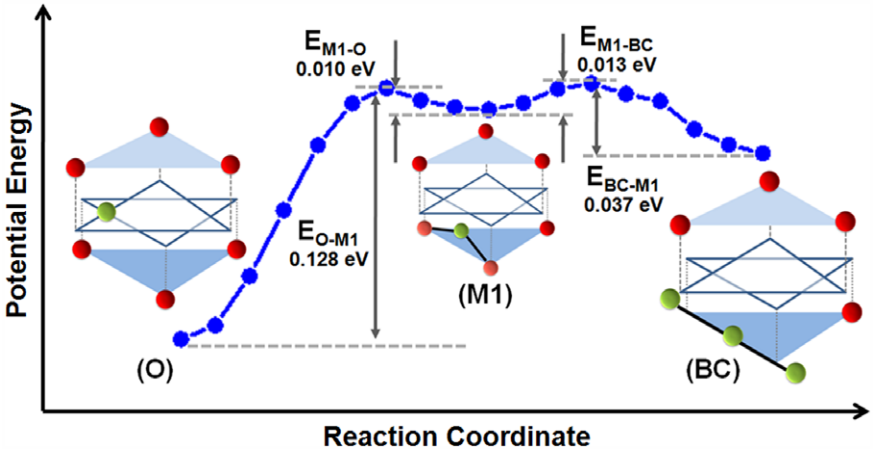

Figure 8. O-M1-BC migration pathway and associated barriers for an SIA from the O state to the BC state. Notice that O-M1 transition actually has a degeneracy of two, although the figure above only shows one of them.

(2.b) *BC-M1-O migration*. The mechanism is just the reverse pathway of O-M1-BC, with a barrier or about 0.04 eV. The configurations and barriers are shown above in figure 8. Notice that the BC-M1 transition has the degeneracy of two, since the middle atom in the crowdion can move either upward or downward.

(2.c) *BC-BO-BC migration*. As shown in figure 10 below, the middle atom in the crowdion migrates to the BO site in the basal plane. The BO site is not stable since the outgoing barrier is only 0.011 eV. Then the BO state migrates to the BC state, with a degeneracy of three. The corresponding migration barriers are also marked in the figure. The effective barrier for such BC rotation is about 0.03 eV.

All the SIA migration mechanisms that were found by ABC-E in hcp Zr are summarized in table 2. We compare the results to Subramanian *et al*'s recent calculations [49] by the TAD method, and most of the mechanisms are found consistently by both the ABC-E and TAD methods, except for the S structure (and its migration paths) which was not considered in this work. The quantitative differences are small, in the range of error tolerance. In general, all the SIA migration barriers were found to be small (0.011–0.131 eV); therefore, SIAs in hcp Zr are expected to exhibit fast diffusion.

In summary, the SIA diffusion in hcp Zr is governed by a mix of 1D and 3D migration mechanisms comprising the following: the O state prefers to hop among the six degenerate neighboring sites in the basal plane with the lowest migration

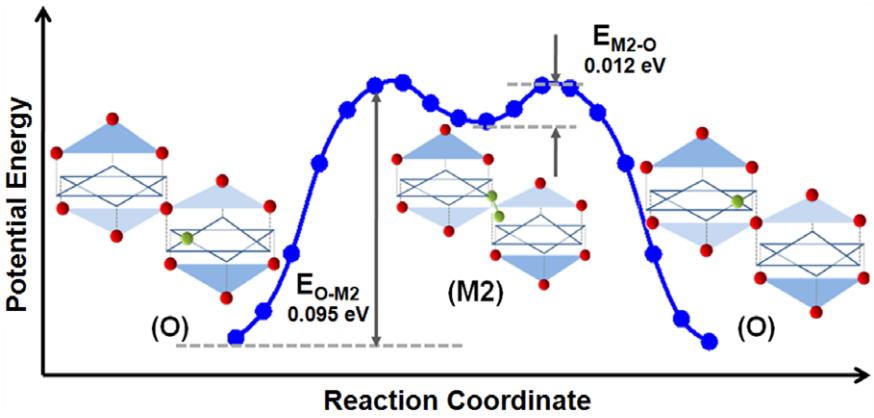

Figure 9. The O-M2-O migration pathway and the associated barriers. O-M2 transition has actually the degeneracy of two, although the figure above only shows one of the transitions.

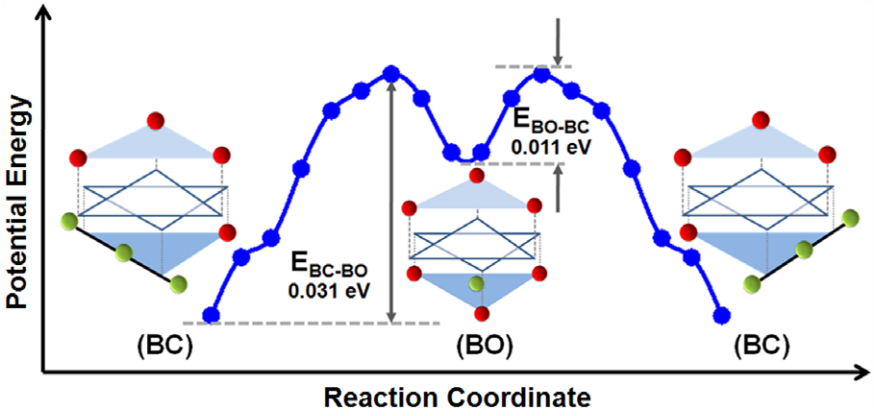

Figure 10. The BC-BO-BC migration pathway and associated barriers for the SIA. BO-BC transition has a degeneracy of three, although the figure above only shows one of them.

Table 2. The summary on the SIA migration mechanisms in hcp Zr modeled by the ABC-E method.

	Migration mechanism	Governing barrier (eV)
O site	O-O (1NN)	0.028
	O-O (2NN)	0.062
	O-M2-O	0.095
	O-M1-BC	0.131
BC site	BC-BC (glide)	0.013
	BC-BO-BC	0.031
	BC-M1-O	0.037
BO site	BO-BC	0.011

barrier. The O state also has some probability to migrate to the O site in a neighboring basal plane via the O-M2-O mechanism, and thus overall would exhibit a 3D migration combining in-plane and out-of plane diffusion. In addition, the O state has a chance to evolve into the BC state via the O-M1-BC mechanism. Once the SIA transits to the BC state, the SIA migration will be mainly governed by the 1D glide motion in the basal plane with the smallest barrier. The BC state also has a probability to transform to another BC state along another direction in the same basal plane, via the BC-BO-BC mechanism. The BC state can jump back to the O state via the BC-M1-O mechanism. Overall, the O-M2-O mechanism provides a 3D motion, while the BC glide provides a 1D motion in the basal plane. The fraction of the 1D and 3D motion can change as a function of temperature because of the different activation energies of these mechanisms. Finally, we would like to note that the activation energies for the BC and BO mechanisms are very small (equivalent to less than 400 K). As a result, at temperatures higher than 400 K, the BC and BO mechanisms can be washed out by thermal fluctuation, and it would not be possible to resolve the different pathways. In the following part of this paper, when discussing the kinetics, we first assume the transition state theory is valid through the entire temperature regime, and then comment on how the kinetics would differ if the thermal fluctuations were to erase the mechanistic details.

4. Anisotropic point defect diffusion kinetics in hcp Zr

4.1. Vacancy diffusion kinetics

The derived mechanisms and barriers and the hcp geometry for the vacancy migration are fed into the kMC model to simulate the diffusion kinetics. In the kMC simulation, we trace the coordinate of the vacancy as a function of the hops it makes in and out of the basal plane. Following the Arrhenius law, the vacancy migration rates in-plane and out-of-plane can be expressed as $k^a = k_0^a \exp[-E_{M1}/k_BT]$ and

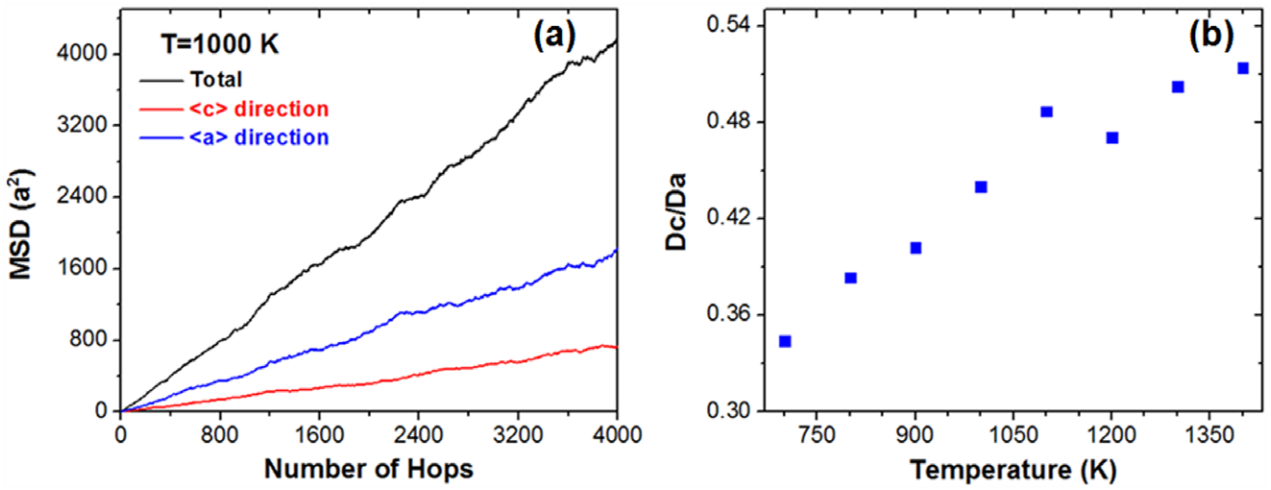

Figure 11. (*a*) The total MSD for vacancy migration and its projection on the <a> and <c> directions in hcp Zr at 1000 K. The total MSD is defined as $MSD_{tot} = \left\langle r_x(t)^2 + r_y(t)^2 + r_z(t)^2 \right\rangle$, where *x*-*y* plane represents the basal plane and *z* represents the <c> direction. The MSD in <a> direction is therefore calculated as $\langle r_x(t)^2 \rangle$, and the MSD in <c> direction is calculated as $\langle r_z(t)^2 \rangle$. The unit of MSD is the square of the lattice parameter on the basal plane, a^2. It can be seen that $MSD_{tot} \approx 2MSD_{<a>} + MSD_{<c>}$. (*b*) The ratio between the diffusivities along the <c> and <*a*> directions (Dc/Da) at various temperatures. All the results in (*a*) and (*b*) are based on the assumption that the pre-factors in the hopping rate of the two paths are the same.

$k^c = k_0^c \exp[-E_{M2}/k_BT]$, respectively. With the assumption that both migration paths have the same pre-exponential factor, i.e. $k_0^a = k_0^c$, we then calculate the mean square displacement (MSD) of the vacancy, including the total MSD, <a> MSD (in-plane) and <c> (out-of-plane) MSD. The total MSD is defined as $MSD_{tot} = \left\langle r_x(t)^2 + r_y(t)^2 + r_z(t)^2 \right\rangle$, where *x*-*y* plane represents the basal plane and *z* represents the <c> direction. The MSD in <a> direction is therefore calculated as $\langle r_x(t)^2 \rangle$, and the MSD in <c> direction is calculated as $\langle r_z(t)^2 \rangle$. The unit of MSD is the square of the lattice parameter on the basal plane, a^2. Figure 11(*a*) shows a typical MSD plot at 1000 K. It can be seen in figure 11(*a*) that $MSD_{tot} \approx 2MSD_{<a>} + MSD_{<c>}$. Furthermore, the slope of <a> MSD is steeper than that of <c> MSD, which indicates an anisotropically favored diffusion kinetics on the basal plane compared to out-of-plane. The ratio between the *c*-axis and *a*-axis diffusivities, Dc/Da (which is equivalent to the ratio of the slope of the <c> MSD to the slope of the <a> MSD) as a function of temperature is shown in figure 11(*b*). The Dc/Da being significantly less than unity indicates a significant anisotropy in the diffusion kinetics in the entire temperature range, with the higher temperatures leading to a less anisotropic behavior, as expected. This behavior is qualitatively consistent with Osetsky *et al*'s previous work [41], which used a different EAM potential [55].

4.2. SIA diffusion kinetics

With all the derived mechanisms and associated barriers in section 3, we employ the kMC simulation to study the SIA diffusion in hcp Zr. According to transition state theory, the transition rate can be expressed as $k^i = k_0^i \exp[-E_i/k_BT]$, where E_i and k_0^i are the reaction barrier and the pre-exponential factor, respectively. In our kMC simulations, all the transitions are assumed to have the same pre-exponential factor, i.e. $k_0^i \equiv k_0 = 10^{13}\text{s}^{-1}$.

4.2.1. SIA diffusion trajectories. Starting from the origin at (0,0,0), the positions of the SIA are traced as a function of time. Figure 12(*a*) shows two SIA diffusion trajectories up to 100 ps, at the temperatures of 300 K and 500 K.

It can be seen from figure 12(*a*) that the diffusion trajectories consist of 'nodes', which are connected by line segments. From the projections on the basal plane (figure 12(*b*)), it is clear that the 'nodes' are in the form of hexagons, which represent the direct O-O hopping mechanism on the basal plane. The short line segments connecting the neighboring hexagons are the O-M2-O migrations, while the long segments are the 1D motion via BC-BC glide mechanism.

4.2.2. Mean square displacement (MSD) of SIA diffusion. The mean square displacement (MSD) of the self-interstitial atoms is calculated similarly to the vacancy MSD described above. Notice that the interstitial atom being traced during the MSD simulations is not necessarily the same initial interstitial atom, because the O-M2-O mechanism is an interstitialcy mechanism and actually switches the initial interstitial atom with a lattice atom. In other words, overall, the MSD of the mass transport is being calculated here, from 100 K up to 900 K. The statistics have been demonstrated to be extremely important in calculating the diffusivities [56]. In this work, to increase the statistics, under each temperature 1000 kMC simulations were employed. In each kMC simulation, we collected the MSD data until 10 ns.

Figures 13(*a*)–(*c*) show the average MSD plots over 1000 kMC simulations, at 150 K, 600 K, and 900 K, respectively. It can be seen from the figure that the slope of <a> MSD is slightly steeper than that of <c> MSD. The ratio between the *c*-axis and *a*-axis diffusivities, Dc/Da, is above 0.8 for the

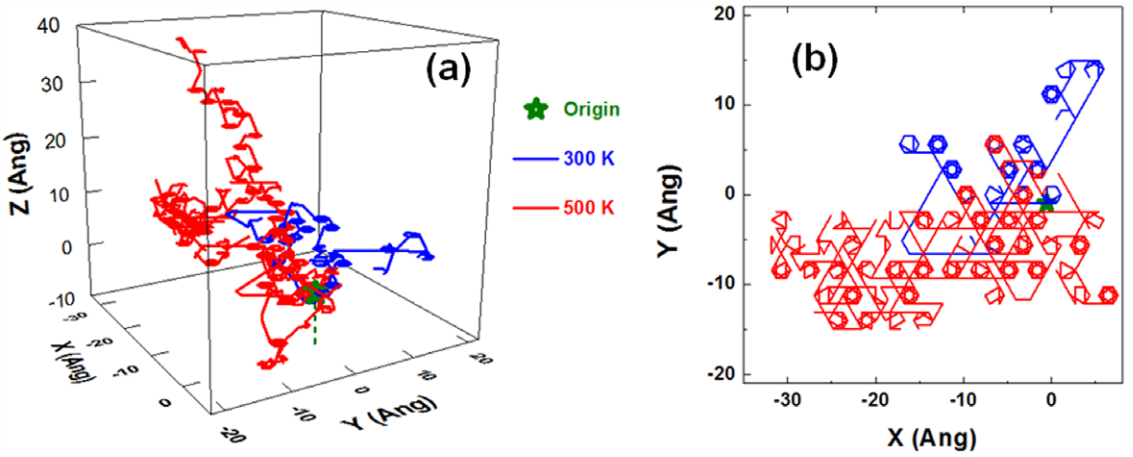

Figure 12. (*a*) SIA diffusion trajectories up to 100 ps at 300 K and 500 K. (*b*) The projections of the trajectories from (*a*) on the basal plane.

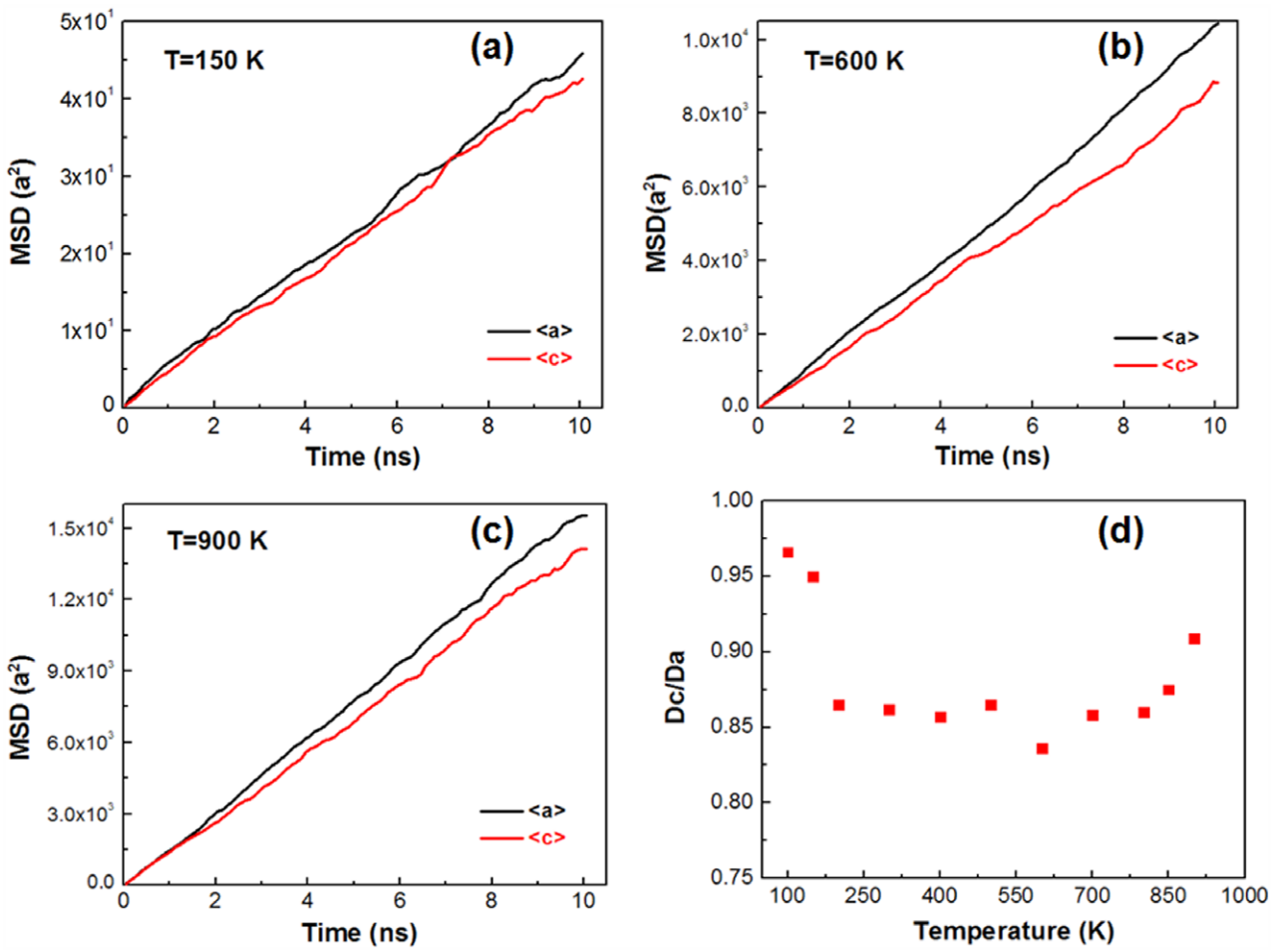

Figure 13. (*a*)–(*c*) The MSD along the <a> and <c> directions at 150 K, 600 K, and 900 K. (*d*) The ratio between the diffusivities along the <c> and <a> directions at various temperatures.

entire simulated temperature range, which indicates that the anisotropic effect is weak (figure 13(*d*)). On the other hand, the plot in figure 13(*d*) shows a very interesting non-monotonic behavior; at the low temperature ($T < 175$ K), diffusion is more isotropic, contrary to the behavior of vacancy diffusion. At intermediate temperatures (175 K < T <600 K), the anisotropy increases as a function of temperature, with Dc/Da decreasing to 0.83.When the temperature is higher than 600 K, the anisotropy decreases as a function of temperature, with Dc/Da again increasing towards 1.00.

Although all the mechanisms introduced in section 3 contribute to the diffusion along the <a> direction, the motion along the <c> direction can only arise from the O-M1-BC and O-M2-O mechanisms. Therefore, the diffusivity along the <c> direction, D_c, is a good indicator of the diffusion mechanisms at different temperatures. In figure 14 we plot D_c

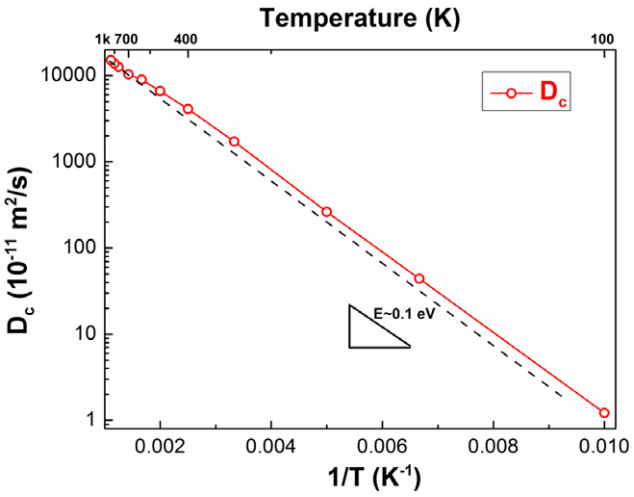

Figure 14. The calculated diffusivity along the <c> direction at different temperatures. The effective barrier is ~0.1 eV.

as a function of temperature. It can be seen that the overall behavior fits well into an Arrhenius manner, with the effective barrier around 0.1 eV, which is a reflection of the O-M1-BC and O-M2-O mechanisms. (See table 2.) However, in the intermediate temperature regime between 400 K and 700 K, the slope of the curve is smaller (a lower barrier), which means the increase of D_c is slower with temperature in this regime.

The non-monotonic behavior in figure 13(*d*) and the slow increase of D_c at intermediate temperatures in figure 14 originate from the temperature dependence of the stability of the SIA site, which favors the O site at the lower temperatures. As shown in table 1, within the MA07 potential, the O state has lower formation energy than the BC state by about 0.1 eV. On the other hand, the O-M2-O mechanism has a lower migration barrier than the O-M1-BC mechanism by about 0.035 eV. Therefore, at low temperatures, the system mostly stays at the O state, and the diffusion is governed by the O-M2-O mechanism, which displays a 3D diffusion and is more isotropic. As the temperature increases, the system has a higher probability to stay at the BC state. For the BC mechanism, as discussed above, the BC-BC glide has a lower barrier than the BC-M1-O migration. Therefore, the fraction of 1D motion, i.e. the anisotropy, starts to increase. This explains the reason for the slow increase of D_c between 400 K and 700 K in figure 14. At high enough temperatures, the differences between all the transitions become insignificant, and the diffusion approaches an isotropic pattern.

The non-monotonic behavior shown in figure 13(*d*) is in contrast to a previous report [41], which shows a monotonic increase of isotropy as a function of temperature. The interatomic potential is a critical factor that leads to the apparent difference in the results here compared to those in [39]. In [39], Osetsky *et al* used the AWB95 potential [55], which predicted the BC state to have the lowest formation energy [53]. Therefore, at the lower temperatures, too, the system has the highest probability of staying at BC state (in contrast to the O-site predicted by the MA07 potential in this work), and thus displays a 1D diffusion mechanism [41]. The 1D diffusion will monotonically transition to a 3D diffusion at high temperatures. In this study, however, with the MA07 potential that predicts the O site to be the most stable, the dominant O mechanism is a 3D migration, as discussed in section 3. Therefore, the system shows a 3D diffusion at the low temperatures. When the temperature increases, the system has a higher probability of staying at the BC state, shifting the diffusion mechanisms toward the 1D motion with increased anisotropy. At higher temperatures, all transitions are effectively activated and the system shows a 3D diffusion with less anisotropy again.

It is worth noting that it is not possible to compare quantitatively our simulated kinetic results (shown in figure 13(*d*)) one-to-one with experiments because of the very small energy barriers involved in some of the identified migration pathways. The mechanisms with low activation energies (e.g. BC and BO) will be indistinguishable at temperatures higher than 400 K. However, the qualitative isotropic-anisotropic-isotropic transition behavior is still expected to remain in general across the temperature range. This is because at low temperatures, where the transition state theory is valid, the system has a higher probability of staying at the BC state as temperature increases, which leads to a higher fraction of 1D motion with increased anisotropy. The isotropic-to-anisotropic transition is thus retained. On the other hand, at high temperatures, where the transition state theory fails, the diffusion becomes more isotropic because the mechanisms become indistinguishable compared to random thermal vibrations. Therefore, the anisotropic-to-isotropic transition is also retained, although this transition could happen earlier at lower temperatures than in figure 13(*d*).

5. A demonstration of the sampling order and computational efficiency of ABC-E

In this section, we show an illustrative example of the comparison between the ABC-E method and ART, in terms of their capability of finding the low-energy saddles with higher probability and their computational expense. The vacancy hopping in HCP Zr, shown above in section 3, is a good example, because all the pathways are known. In particular, there are two migration pathways: the in-plane (M1) and out-of-plane (M2) paths. The in-plane hopping, M1, has a lower barrier (0.68 eV) than the out-of-plane hopping, M2 (0.76 eV), and both pathways have a degeneracy of six. Therefore, in total there are 12 pathways, and the perfect order of finding these from the lowest to the highest energy barriers would be: M1, M1, M1, M1, M1, M1, M2, M2, M2, M2, M2, M2.

By the ABC-E method, with the penalty parameters of 0.5 eV, 0.25 A^2 (for both the bias filling function and the blocking function), all 12 pathways are identified within 86 steps. Each step in the ABC-E method consists of 500 force evaluations, and the total computation involves 43 000 force evaluations. The order of pathways identified by ABC-E is: M1, M1, M1, M2, M2, M1, M2, M1, M1, M2, M2, M2 (shown below in figure 15). It can be seen that the general trend of increasing order (from paths with low barriers to those with high barriers in the search) is retained. Admittedly,

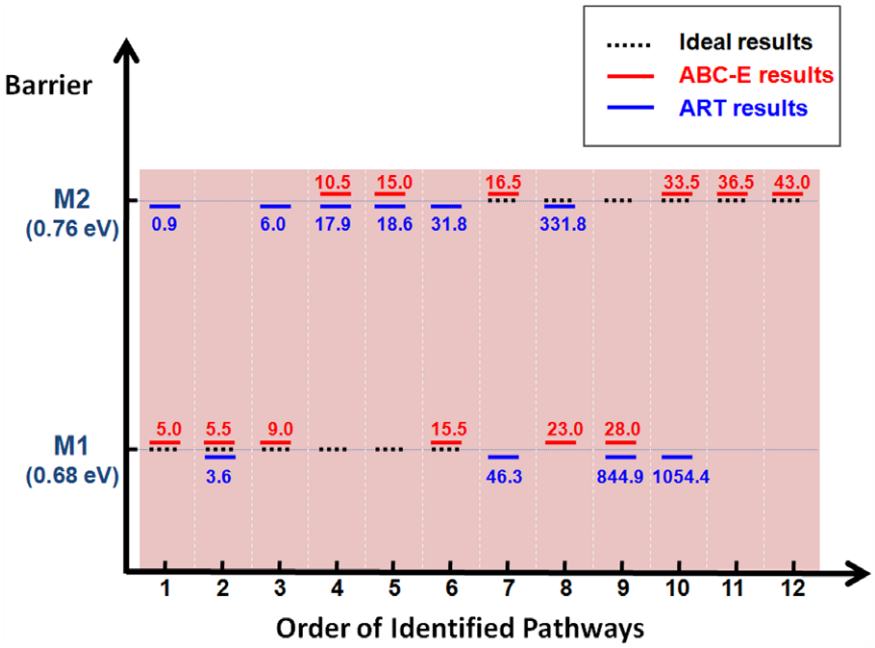

Figure 15. Results of the identified pathways by the ABC-E method and ART for vacancy migration in hcp Zr. In ABC-E, all 12 pathways are identified in a sequence approximately, with increasing migration barrier energy (M1, M1, M1, M2, M2, M1, M2, M1, M1, M2, M2, M2). In ART, within 500 searches, 10 different pathways were identified, and the order of the found pathways appears random (M2, M1, M2, M2, M2, M2, M1, M2, M1, M1). The values next to the bars represent the number of force evaluations (in units of ×1000), up to which the corresponding pathway is identified for the first time.

local reverse-finds exist because the saddle point energy differences are quite small compared with the height of the penalty function used in ABC-E.

We also searched for the migration paths for vacancy in hcp Zr by using ART as implemented in the code developed by Mousseau *et al* [57]. In the search, the magnitude of initial displacement was set as 0.1 Å, and the direction was randomly chosen. When the curvature of the underlying potential energy surface was found to be less than $-2\,\mathrm{eV/Å^2}$, the system was relaxed to the saddle point using the Lanczos algorithm. The saddle point convergence criterion was fulfilled when the overall force of the total system was less than 0.05 eV/Å. Starting from the same initial configuration, we tried 500 searches with ART, which included 1 158 112 force evaluations in total. During these 500 searches, some results were unreasonable because they were climbing the PES too high (as also noted in [12]), and some pathways were revisited many times (as discussed in [48]). On the other hand, not all the 12 pathways were identified. In particular, 10 different pathways were observed, and two of the M1 pathways were missing from the 500 searches (as shown in figure 15). The order of 10 identified pathways by ART is: M2, M1, M2, M2, M2, M2, M1, M2, M1, M1. We noticed that there were reported observations that low energy saddles were more easily identified by ART [48]. However, as seen in figure 15, there is no clear order in the sequence of the pathways found by ART in this problem. We think the previous observation in [48] is empirical as there is no underlying algorithmic reason within ART for finding the pathways with increasing order of barrier heights.

The computational costs of ABC-E and ART are also shown in figure 15. It took 43 000 force evaluations for ABC-E to identify all 12 pathways. On the other hand, with a total of 1 158 112 force evaluations, 10 different pathways were identified by ART. Another appealing feature of ABC-E is that different searches are not completely independent of each other. In particular, once the first pathway is observed, the successive searches do not start from the very bottom of the basin. Instead, the successive searches start from the current level of the partially filled basin. This procedure makes the sampling more efficient. As seen in figure 15, although it takes 10 steps (5000 force evaluations) to find the first pathway, all 12 pathways are identified in 86 steps (43 000 force evaluations). This shows a noticeable increase of efficiency in the later stages of sampling in ABC-E. On the other hand, with the same problem solved by ART, the numbers of force evaluations in different searches are always independent of each other, with an average number of force evaluations per search of about 2316 (the total force evaluations 1 158 112 divided by 500 searches). As can be seen in figure 15, ART takes less time than ABC-E in finding the first three pathways. However, as the samplings continue, ART suffers the problem of redundant visits [48], which makes it less efficient than ABC-E overall. Particularly in this example, it took 43 000 force evaluations for ABC-E and 1 158 112 force evaluations ART, respectively, meaning ABC-E is at least 25 times more efficient than ART (as ART did not find the complete set of paths within this search set).

In spite of the comparison shown above, we believe different modeling techniques have their own features that are particularly applicable to different problems. For example, ART and the Dimer method are demonstrated to be highly accurate in problems where the dynamics of multiple objects are involved [13, 15–19]. The original ABC method has been demonstrated to be particularly robust in revealing the

underlying mechanisms for unit processes [22, 26, 29]. The current ABC-E method extends the accuracy of the original algorithm from unit processes to problems where the dynamics of multiple objects are involved. Undoubtedly, every technique has its own advantages and shortcomings. Future work benchmarking the similarities, differences, and consistencies among techniques on a variety of problems should prove useful for the computational materials community.

6. Conclusions

Here we presented an extension of the ABC algorithm, called ABC-E, to improve accuracy in predicting the kinetics of complex system evolution while retaining efficiency. Specifically, the ABC-E algorithm permits the sampling of multiple transition pathways from a given minimum energy state on the potential energy landscape, contrary to the 1D system evolution exhibited by the original ABC algorithm. When a transition pathway is found using the original ABC algorithm, a blocking penalty function is added onto the saddle point, and the system is set back to the original given basin. By performing this procedure iteratively and choosing the blocking and search criterion carefully, a series of transition pathways associated with the given basin can be identified. We demonstrated on a hypothetical PES that the combination of ABC-E and on-the-fly kMC calculations allows a significantly more accurate description of the kinetics of system evolution, matching that of the full catalogue kMC results. By comparing ABC-E and the ART method in the simulation of vacancy migration in hcp Zr, we have also demonstrated the prioritization of sampled paths in the order of increasing activation energies. This feature of ABC-E enables computationally efficient importance sampling.

This ABC-E algorithm, in combination with other coarse graining methods, can provide an opportunity to accurately, and relatively efficiently, describe materials' macroscopic behavior in a multi-scale sense. For example, recent related works [29, 58] demonstrate a multi-scale framework for studying the materials' mechanical response to the surrounding environments. Such frameworks require the atomistic mechanisms as input, which were provided by the original ABC algorithm.

In the latter part of this paper, we employed ABC-E to simulate the diffusion of point defects in an anisotropic material, the hcp Zr. This problem makes an ideal physical test bed for ABC-E because point defect diffusion is associated with multiple migration mechanisms that could not be captured by the original ABC algorithm, and because an accurate description of point defect diffusion is important for predicting microstructure evolution in materials of importance to nuclear systems. We demonstrated that the ABC-E method could capture all the multiple migration mechanisms of vacancies and self-interstitial atoms in hcp Zr, consistent with other available results from literature. Combining the mechanisms and barriers identified from ABC-E with on-the-fly kMC simulations, we assessed the temperature dependence of the vacancy diffusion and SIA diffusion kinetics. An interesting, non-linear isotropic-anisotropic-isotropic transition with increasing temperature was found for the SIA diffusion. This behavior originates from the temperature dependence of the stability of the SIA site. The SIA stability favors the O-site at the lower temperatures, and the BC-site competes with the O-site with increasing temperature when using the MA07 interatomic potential in this work. Therefore, at the low temperatures, the diffusion is governed by the O-M2-O mechanism, which displays a 3D diffusion and is more isotropic. As the temperature increases, the system has a higher probability of staying at the BC state and exhibiting the BC-BC glide motion in 1D with increasing anisotropy. At high-enough temperature, the differences between all the transitions become insignificant, and the diffusion approaches an isotropic pattern. This behavior is different from the previously predicted monotonic increase of isotropy in SIA diffusion kinetics when using the ABW95 potential. We believe the different relative stabilities of the O- and BC-sites predicted by the different interatomic potentials employed are a critical factor that leads to this difference. On the other hand, there is yet no clear experimental conclusion on the relative stability of different SIA sites [50, 51, 59, 60], and this makes it particularly challenging to completely validate the predictions of SIA diffusion in hcp Zr.

There exist a wide variety of problems based on defect evolution and mobility in complex media, which involve time scales well beyond the reach of traditional molecular dynamics simulations. The optimization of the ABC algorithm by Cao *et al* [24] and the ABC-E method presented here are alternative contributions that will allow the resolution of the kinetic mechanisms governing the functional behavior of materials at the mesoscale [61], in addition to other existing atomistic techniques aiming for long time scales.

Acknowledgments

This work was supported by the Consortium for Advanced Simulation of Light Water Reactors, an Energy Innovation Hub for Modeling and Simulation of Nuclear Reactors under US Department of Energy Contract No. DE-AC05-00OR22725. Y F would also like to acknowledge the support of Eugene P Wigner Fellowship at the Oak Ridge National Laboratory, managed by UT-Battelle, LLC, for the US Department of Energy under Contract No. DE-AC05-00OR22725.

References

[1] Crabtree G W and Sarrao J L 2012 *MRS Bull.* **37** 1079
[2] Yip S 2003 *Nat. Mater.* **2** 3
[3] Mansur L K 1994 *J. Nucl. Mater.* **216** 97
[4] Sastry S, Debenedetti P G and Stillinger F H 1998 *Nature* **393** 554
[5] Voter A F 1997 *J. Chem. Phys.***106** 4665
[6] Pal S and Fichthorn K A 1999 *Chem. Eng. J.* **74** 77
[7] Wang J-C, Pal S and Fichthorn K A 2001 *Phys. Rev.* B **63** 085403
[8] Sorensen M R and Voter A F 2000 *J. Chem. Phys.* **112** 9599
[9] Hara S and Li J 2010 *Phys. Rev.* B **82** 184114

[10] Ishii A, Ogata S, Kimizuka H and Li J 2012 *Phys. Rev.* B **85** 064303
[11] Barkema G T and Mousseau N 1996 *Phys. Rev. Lett.* **77** 4358
[12] Cances E, Legoll F, Marinica M C, Minoukadeh K and Willaime F 2009 *J. Chem. Phys.* **130** 114711
[13] Henkelman G and Jonsson H 1999 *J. Chem. Phys.* **111** 7010
[14] Kushima A, Lin X, Li J, Eapen J, Mauro J C, Qian X, Diep P and Yip S 2009 *J. Chem. Phys.* **130** 224504
[15] Xu H, Osetsky Y N and Stoller R E 2011 *Phys. Rev.* B **84** 132103
[16] Haixuan X, Yuri N O and Roger E S 2012 *J. Phys.: Condens. Matter* **24** 375402
[17] Xu H, Osetsky Y N and Stoller R E 2012 *J. Nucl. Mater.* **423** 102
[18] Béland L K, Brommer P, El-Mellouhi F, Joly J-F and Mousseau N 2011 *Phys. Rev.* E **84** 046704
[19] Heyden A, Bell A T and Keil F J 2005 *J. Chem. Phys.* **123** 224101
[20] Kallel H, Mousseau N and Schiettekatte F 2010 *Phys. Rev. Lett.* **105** 045503
[21] Rodney D and Schuh C 2009 *Phys. Rev. Lett.* **102** 235503
[22] Wang H, Xu D S, Rodney D, Veyssière P and Yang R 2013 *Modelling Simul. Mater. Sci. Eng.* **21** 025002
[23] Laio A and Parrinello M 2002 *Proc. Natl Acad. Sci.* **99** 12562
[24] Cao P, Li M, Heugle R J, Park H S and Lin X 2012 *Phys. Rev.* E **86** 016710
[25] Fan Y, Kushima A and Yildiz B 2010 *Phys. Rev.* B **81** 104102
[26] Wang H, Rodney D, Xu D, Yang R and Veyssière P 2011 *Phys. Rev.* B **84** 220103
[27] Fan Y, Osetsky Y N, Yip S and Yildiz B 2012 *Phys. Rev. Lett.* **109** 135503
[28] Fan Y, Kushima A, Yip S and Yildiz B 2014 unpublished
[29] Fan Y, Osetskiy Y N, Yip S and Yildiz B 2013 *Proc. Natl Acad. Sci.* **110** 17756
[30] Brommer P and Mousseau N 2012 *Phys. Rev. Lett.* **108** 219601
[31] Fan Y, Kushima A, Yip S and Yildiz B 2011 *Phys. Rev. Lett.* **106** 125501
[32] Fan Y, Kushima A, Yip S and Yildiz B 2012 *Phys. Rev. Lett.* **108** 219602
[33] Lemaignan C and Motta A 1994 *Materials Science and Technology* **10B** ed B R T Frost (Weinheim: VCH)
[34] Griffiths M 1988 *J. Nucl. Mater.* **159** 190
[35] Griffiths M 1993 *J. Nucl. Mater.* **205** 225
[36] Hayes T, Kassner M and Rosen R 2002 *Metall. Mater. Trans.* A **33** 337
[37] Hayes T and Kassner M 2006 *Metall. Mater. Trans.* A **37** 2389
[38] Voskoboinikov R E, Osetsky Y N and Bacon D J 2005 *Mater. Sci. Eng.* A **400–401** 49
[39] Voskoboynikov R E, Osetsky Y N and Bacon D J 2005 *Mater. Sci. Eng.* A **400–401** 54
[40] Mendelev M I and Ackland G J2007 *Phil. Mag. Lett.* **87** 349
[41] Osetsky Y, Bacon D and de Diego N 2002 *Metall. Mater. Trans.* A **33** 777
[42] Voter A F 2007 *Radiation Effetcs in Solids* ed K E Sickafus, E A Kotomin and B P Uberuaga (Berlin: Springer) 1–24
[43] Bowman G R, Beauchamp K A, Boxer G and Pande V S 2009 *J. Chem. Phys.* **131** 124101
[44] Prinz J-H, Keller B and Noe F 2011 *Phys. Chem. Chem. Phys.***13** 16912
[45] Kushima A, Lin X, Li J, Qian X, Eapen J, Mauro J C, Diep P and Yip S 2009 *J. Chem. Phys.* **131** 164505
[46] Lau T T, Kushima A and Yip S 2010 *Phys. Rev. Lett.* **104** 175501
[47] Li J, Kushima A, Eapen J, Lin X, Qian X, Mauro J C, Diep P and Yip S 2011 *PLoS ONE* **6** e17909
[48] Malek R, Mousseau N and Barkema G T 2001 *Mat. Res. Soc. Symp. Proc.* **677** AA8.4
[49] Subramanian G and Tomé C N 2012 *Technical Report* LA-UR-12-25613
[50] Willaime F 2003 *J. Nucl. Mater.* **323** 205
[51] Domain C and Legris A 2005 *Phil. Mag.* **85** 569
[52] Vérité G, Domain C, Fu C-C, Gasca P, Legris A and Willaime F 2013 *Phys. Rev.* B **87** 134108
[53] Khater H A and Bacon D J 2010 *Acta Mater.* **58** 2978
[54] Peng Q, Ji W, Huang H and De S 2012 *J. Nucl. Mater.* **429** 233
[55] Ackland G J, Wooding S J and Bacon D J 1995 *Phil. Mag.* A **71** 553
[56] Deng C and Schuh C A 2011 *Phys. Rev. Lett.* **106** 045503
[57] http://www.pmc.umontreal.ca/~mousseau/site_an/index.php?n=Main.Software
[58] Cao P, Park H S and Lin X 2013 *Phys. Rev.* E **88** 042404
[59] Pichon R, Bisognis E and Mosek P 1973 *Radiat. Eff.* **20** 159
[60] Ehrhart P and Schonfeld B 1982 *Proc. of Yamada Conference on Point Defects and Defects Interactions in Metals* (*Kyoto, November 1981*) ed V Takamura, J Doyama and M Kiritani p 47
[61] Yip S and Short M P2013 *Nat. Mater.* **12** 774